Ninth International Conference on Computational Fluid Dynamics (ICCFD9), Istanbul, Turkey, July 11-15, 2016

ICCFD9-2016-169

Numerical Validation for Aeroacoustic Transmission Loss Performance of a High Frequency Wave Bypass Filter Based On Destructive Interferometry

Barış Elbüken[1], Alper Ata[1]

[1]Heating Division, Alarko Carrier Research and Development Center, Kocaeli 41480, Turkey

Corresponding author: baris.elbuken@alarko-carrier.com.tr

Abstract: Noise reduction is highly important in any domestic or industrial environment for satisfying acoustical comfort. In fluid intake or exhaust nozzles, it is foreseen to passively reduce ear disturbing noise by using destructive interferometry of the waves emitted by the in duct located sound source is possible. The formerly designed tunable high frequency filter is expected to perform highest success of transmission loss in a related tune position. The numerical validation approach stated in this paper is on a source oriented passive filtering method implementation that takes a curved bypass duct as a silencer. The acoustic transmission losses without fluid flow and also in mean flow are examined numerically on Elbüken's Acoustic Filter (EAF). Time domain responses to perturbing inlet noise has been recorded and transformed to frequency domain responses by using a Characteristics Based Filter (CBF) and Fast Fourier Transformation (FFT) in order to calculate the scattering matrix coefficients.

Keywords: Aeroacoustics, Passive Sound Filtering, Destructive Interferometry, LES, CBF, Transfer Matrix, Scattering Matrix, Acoustical Signal Processing.

1 Introduction

Experiments being conducted on a wall hung condensing gas boiler concentrating on detecting the premixed combustion lean and rich limits aroused a disturbing noise of ~2 kHz with a narrow bandwidth which has been concluded as a sharp disturbing noise for the user/operator. Depending on the so called disturbance, in order to satisfy acoustical comfort requirements, successive performance of an aeroacoustical destructive interferometric sound filter capable of being tuned to a desired frequency of interest has been designed and patented due to the results documented in this paper.

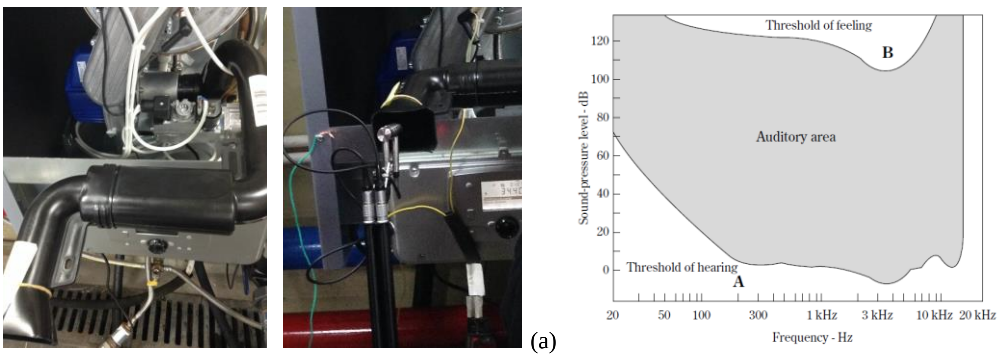

(a) (b)

Figure 1: (a) Laboratory test setup used in acoustical measurements, (b) human audiogram [2].

The human audiogram is seen in Figure 1. It is clearly seen that the human ear is mostly sensitive to high frequency sound waves of kHz order of magnitude. Regarding the so called uncomfortable sound of ~2kHz frequency with peak amplitude falls just below the very close region of most sensitive region.

2 Methods

2.1. Governing equations

In order to determine the time evolution of the aero-acoustical physical system of interest, it is needed for the three fundamental equations to be soled whether analytically or numerically to interpret results. The below equations are the continuity equation, the combined Navier-Stokes equation neglecting the gravity terms [3] and acoustical wave equation [4] which is governing the acoustical propagation which can be found in numerous textbooks.

$$\frac{D\rho}{Dt} + \rho\vec{\nabla}.\vec{V} = 0 \tag{1}$$

$$\frac{D\vec{V}}{Dt} = -\frac{1}{\rho}\vec{\nabla}P + \frac{\partial}{\partial x_j}\left[\mu\left(\frac{\partial u_i}{\partial x_j} + \frac{\partial u_j}{\partial x_i}\right) - \delta_{ij}\frac{2}{3}\mu\vec{\nabla}.\vec{V}\right] \tag{2}$$

$$\frac{\partial^2 P}{\partial x_j^2} = \frac{1}{c^2}\frac{\partial^2 P}{\partial t^2} \tag{3}$$

The wave equation is given for a single dimension thus it could be stated in the compact form as $c^2\left(\nabla^2 P\right) - \ddot{P} = 0$ also.

2.2. Destructive interferometry: An advantage

In the nature, there are numerous examples of the interference of waves. The wave, is known as its bahaviour, is a linear convex combination of any oscillating physical observable in harmonic spatial and time evolution. The uneven surface of seas is a good example. Every single unit part of the surface tends rising or lowering in the normal direction to earth with different behaviors also with time dependence.

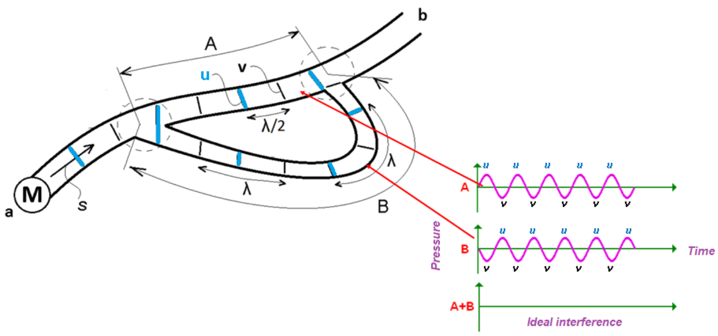

Figure 2: Successive splitting and recombination of sound waves in a bypass duct system.

In any fluid conveying duct like air intake or exhaust nozzles etc., the propagating wavefronts emerging from a source like a fan or motor (M) can be split into a secondary ductway in order to recombine with the original duct wavefront in a position different than the splitting node. As well as the pathway difference being appropriate, a corresponding component of the complex sound wave will obey the rule to destructively self interfere at the recombination (rendezvous) location producing a net wave with a reduced amplitude. This is the main idea behind the design in the focus of this paper.

The success of destructive interference is maximum with a zero resultant (superposed) wave amplitude. The wave propagation may be influenced by internal reflections and the splitting and recombining waves may have phase changes between the two. With zero reflecting walls, phase change can not be counted due to a reflecting oriented event thus may the condition of successive destructive interference be expressed as in the first line of Eq (4) where m is a positive integer. In the contrary, with fully reflecting walls, internal reflections can produce the successive destructive interference with the 2nd line of Eq (4).

$$|B-A| = \Delta S = \begin{cases} (2m+1)\dfrac{\lambda}{2} \quad ,in-phase & \\ & m = 0,1,2... \\ (m+1)\lambda \quad ,out \;\; of \;\; phase & \end{cases} \tag{4}$$

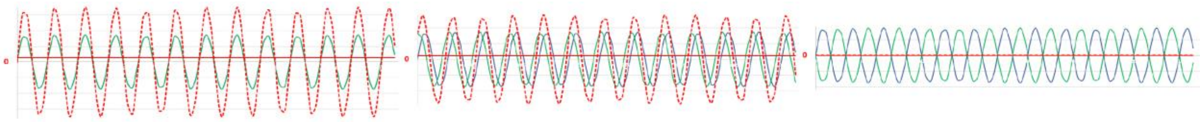

(a) (b) (c)

Figure 3: Interference of monochromatic waves for three different relative phases: Resultant wave denoted by thick red line (a) worst case: gain occured, (b) poor success: limited gain occured, (c) success: ideal case with zero resultant wave.

Any acoustical wave transfer medium including a main passage and a secondary passage which are connected to each other by two nodes of interaction is due to the so called interference phenomena. The curvilinear path length difference (*ΔS*) will always satisfy a destructively self-interfering wave component of wavelength λ at the rendezvous node as in Eq (1) where m is a positive integer. This wave component is the one with maximum transmission loss (*TL*) in the filter assembly's current position. With a selected path difference, the maximum filtered expected frequency is dependent on the tuned pathway difference and the local speed of sound in the medium.

2.3. Acoustical signal processing

The method for analyzing the consequences of duct flow aeroacoustics also in case of fluid flow has been studied in detail by numerous researchers. Kopitz et. al. [5] has proposed an intelligent way of filtering LES mean flow data from the flow solution by using a method which they call Characteristics Based Filter (CBF). It is an advantage declared by them is that the CBF method can be applied during the numerical simulation in real time as well as in post processing phase which is counted by them applicable universally.

Föller and Polifke [1] have used a method for filtering and identifying acoustical data gathered from an LES mean flowfield solution for a sudden area expansion in a circular duct by the CBF method of Kopitz et. al. [5]. They also have implemented a hybrid computational fluid dynmics + system identification (CFD/SI) approach to be able to identify the acoustical system behaviour with an only single LES simulation.

In order to process time series data taken from a mean flow LES data, the CBF offered by Kopitz et. al. [5] and occupied by Föller and Polifke [1] in their circular duct research is used. In the below equations c is the local speed of sound, and k is the "order number" of the data monitoring/recording points with $\bar{u}$ being the mean flow speed of the fluid. p^{+}_{CBF} and p^{-}_{CBF} are the filtered pressure wave amplitudes extracted from the flowfield.

$$p^{\pm}_{CBF}(x,t) = \frac{1}{n}\sum_{k=0}^{n-1} p^{\pm}_{k}\left(x - k\Delta x, t \mp \frac{k\Delta x}{c \pm \bar{u}}\right) \tag{5}$$

Time series acoustical static pressure data with propagation direction has been achieved by using down/upstreamwise CBF'd pressure data also with the mean flow field speed.

$$\hat{p}^{\pm}_{u/d} = \frac{1}{2}(\hat{p}^{'}_{u/d} \pm \rho c \hat{u}^{'}_{u/d}) \quad \textbf{(6)}$$

The transfer and reflection coefficients ($T^{\pm}$, $R^{\pm}$) can be quantified by using the transformation with the acoustics data forming the transfer matrix.

$$\begin{pmatrix} \hat{p}^{+}_{d} \\ \hat{p}^{-}_{u} \end{pmatrix} = \begin{pmatrix} T^{+} & R^{-} \\ R^{+} & T^{-} \end{pmatrix} \begin{pmatrix} \hat{p}^{+}_{u} \\ \hat{p}^{-}_{d} \end{pmatrix} \quad \textbf{(7.1)}$$

By means of velocity scale, the so called matrix is written as the scattering matrix notation with C_{ij} being the scattering coefficients.

$$\begin{pmatrix} \dfrac{\hat{p}^{'}_{i}}{\rho c} \\ \hat{u}^{'}_{i} \end{pmatrix}_{d} = \begin{pmatrix} C_{11} & C_{12} \\ C_{21} & C_{22} \end{pmatrix} \begin{pmatrix} \dfrac{\hat{p}^{'}_{i}}{\rho c} \\ \hat{u}^{'}_{i} \end{pmatrix}_{u} \quad \textbf{(7.2)}$$

$\hat{p}_u$ and $\hat{p}_d$ being generally the incident and transmitted pressure wave amplitudes, transmission loss (TL) is calculated as in the below equation which was also used by Middelberg et. al. [6].

$$TL = 20\log_{10}\left(\frac{\hat{p}_u}{\hat{p}_d}\right) \quad \textbf{(8)}$$

In addition to Eq (8), as derived and introduced by Noreland [8] the negative value of the C_{12} element corresponds to the acoustical impedance which can be written in terms of the acoustical resistance (Z_r) and acoustical reactance (Z_I) as follows.

$$Z = -C_{12} = \frac{\hat{p}^{'}_{u} - \hat{p}^{'}_{d}}{\rho c \hat{u}^{'}_{u}} = Z_R + iZ_I \quad \textbf{(9)}$$

2.4. Filter design and tuning mechanism geometry

The basic functionality of the filter design is to be able to filter the disturbing acoustical noise corresponding to the relative path difference between the assembly pathways. Hwang et. al. [10] have made an efficient work on a new destructively interfering active muffler. In their attempt, they have formerly underlined the powerful effect of destructive interference also without needing any external energy source as in active sound filtering methodologies. Their work involves numerical and experimental efforts with the implementation on a four-cylinder 2.0l gasoline internal combustion test engine and focuses mainly on low frequency components emerging from combustion. They have proposed a new method for exhaust noise control with U-shaped bypass pipe which is attached to the main flow ductline. It is stated in their work that in low rpm (thus frequency) regime, passive muffler, and for the high rpm range their proposed U-shaped muffler is employed which has achieved more than 20 dB decrease on their sound components in focus (low frequency).

It is an important disadvantage of Hwang et. al. [10] design is it's huge size and difficulty to be implemented on a passenger car or any domestic heating appliance like a wall hung boiler etc. So forth, a tunability for the pathway difference can better be adapted with different mechanisms and for different frequencies of interest. An efficient way to easily tune, a new filter mechanism and method by the corresponding author is also introduced here.

The filter structure is composed of three main parts. An outside shell with a spiral secondary pathway, an inner shell with an axially aligned slit and lastly a sliding seperator. The assembly is introduced below.

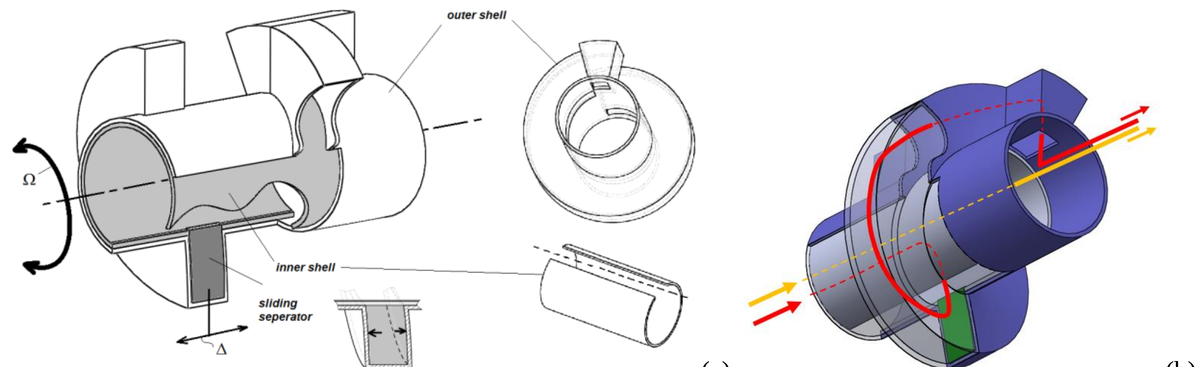

(a) (b)

Figure 4: Destructive interferometric filter (a) assembly and sub components, (b) method of operation.

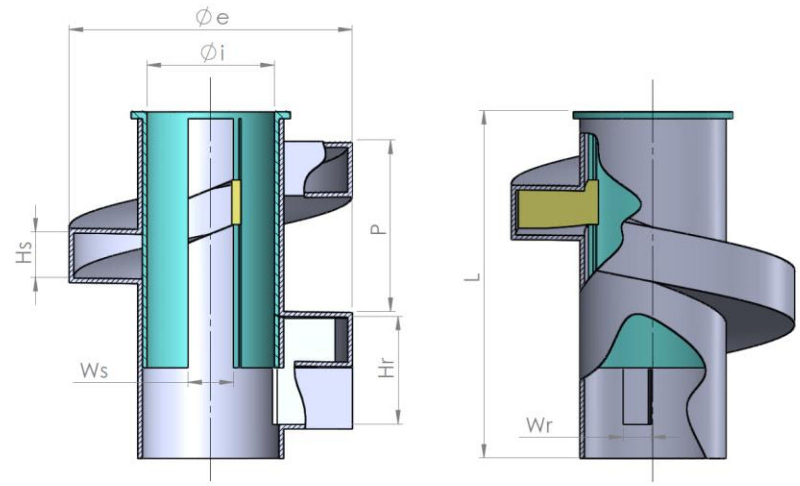

Figure 5: Filter main dimensions.

Table 1: Main dimensional values.

Dimension	**Symbol**	**Value**
External diameter	ϕ_e	124 mm
Internal diameter	ϕ_i	56 mm
Pitch	P	76 mm
Room height	H_r	47 mm
Room gate width	W_r	12,8 mm
Spiral cross section height	H_s	20 mm
Slit width	W_s	20 mm
Total height	L	153 mm
Outer shell thickness	t_o	2 mm
Inner shell thickness	t_i	2 mm

With the aid of the relative circumferal displacement (Ω) between the inner and outer shells, the sliding seperator is forced to maintain its position between the inner shell slit and the outer shell's spiral duct surrounding, thus resulting with a relative linear motion (Δ) on the inner shell slit's side (like a linear bearing). By this way, the relative path difference can be tuned with a relative rotational motion.

When determining the filter assembly geometry of interest, the first mode interference (with m=0) is taken into account. In order to achieve a worst case disturbing noise handling, the filter is dimensionalized with the corresponding order of magnitude. The local speed of sound is taken to be c=346 m/s. The pathway difference (ΔS) is the same order of magnitude with the filter length or external diameter. Someone knows the relationship between the wave frequency (f) and the wavelength (λ) is $c = f.\lambda$ thus, taking the frequency magnitude as $[f] \approx 10^3$ Hz, this corresponds to the filter dimensions' order of magnitude. $[\boldsymbol{\lambda}] \approx [\Delta S] \approx [\boldsymbol{L}] \approx 10^{-1}$ m. It would not be abnormal to state that, the filter with this order of magnitudes would be beneficial for high frequencies (kHz) of interest.

2.5. Boundary conditions and computational mesh

The problem geometry is designed as seen below. An air intake diffuser is open to far field pressure boundary condition which is nearly 20 m equidistant from the pipe end. The domain structure is a semi sphere with radius to which the air suction side is 16 diameters far from the filter and the center of the semi sphere 5 diamaters. One of the capabilites of the solver software CFX is that, in cases that the user has a a difficulty on whether the outlet boundary pressure acts like a temporary inlet (i.e. backflow from the boundary) then, the code self tunes to act like total pressure thus taking the temporal value of the static pressure component to a lower value. In the contrary, when the temporal flow is outwards, the pressure boundary acts as a static pressure boundary. This is also called in the CFX literature as the "opening boundary condition" [7].

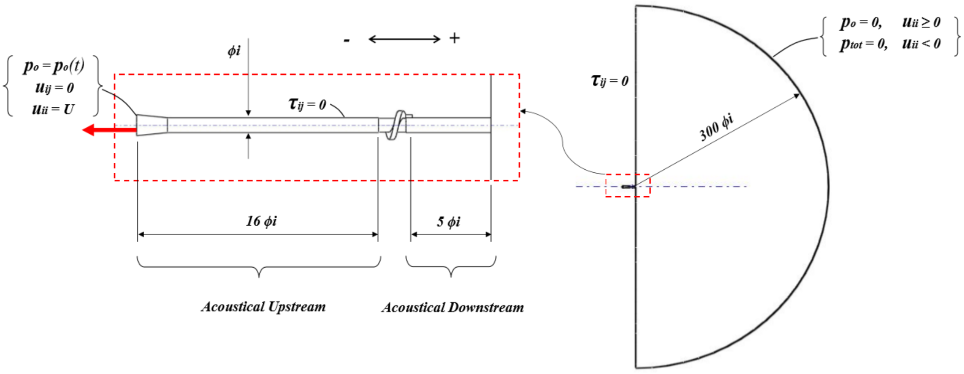

Figure 6: Boundary conditions and the posed problem.

In Figure 6 it is seen that, the flow outlet is also the acoustical perturbation side, emitting planar pressure waves towards the semi sphere center. It will furtherly be explained in the latter portions of the text but the simulations are consisting of 1) only acoustical perturbation and 2) acoustical perturbation plus mean fluid flow. For the sake, the acoustical perturbation side is also consisting a velocity outlet condition. Namely, the upstream side for the duct flow is the "acoustical downstream" and substitutively the flow downstream side is the "acoustical upstream" side respectively.

Middelberg et. al. [6] have conducted a research on an expansion chamber muffler sound attenuation concluded that for lower frequencies below 1,5 kHz the, numerical simulations show close agreement with each other. For frequencies above 1,5 kHz, the mesh resolution has an influence on the solution. For the CFD produced acoustic results generated with a mesh size of 4 mm per a unit edge length is concluded to give a good compromise between solution time and accuracy. For the maximum frequency of their interest (3 kHz) this relates to ~28 cells per wavelength for their 4mm per edge length square mesh.

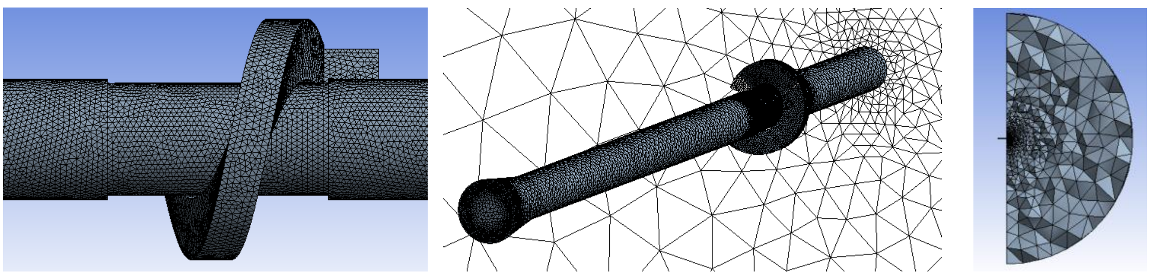

Figure 7: Computational mesh of the flow domain.

In Dykas et. al. [9], it has been shown that 5 nodes per wavelength has accurate results predicted by an Euler Acoustic Postprocessor (EAP) in comparison with analytical results. In the same work, in order to get accurate results for time-dependent pressure distribution on solid bodies, on a cylinder and on a profile they have selected the numerical mesh is said to be created to preserve at least 10 mesh points per acoustic wavelength, for getting satisfactory results by their EAP method with their former works.

It has been shown by Föller and Polifke [1] that, to be able to well resolve the acoustical wave behaviour, 50-70 cells per wavelength should be assigned for the domain of interest. Taking these results into account, minimum of 50 elements per wavelength has been occupied to discretize the flow domain.

2.6. Numerical method

In case of acoustic waves, unstructured meshes are regarded useful depending on the isotropic nature of wave propagation neither than a directed alignment. An unstructured mesh (~300k elements) fine enough and timestep sizes small enough have been used to satisfy the node-per-half wavelength accuracy needs (~25 nodes per half-wavelength) for both time and space domains and also the LES turbulence model subgrid scale resolution. High resolution advancing scheme for space and 2nd order backward Euler advancing scheme in time are implemented for the equations.

Numerical simulations have been conducted in Ansys CFX 14.5 code on a multiprocessor workstation via parallel processing. CFX is a density based compressible flow finite volume solver. SIMPLE algorithm has been utilized for pressure-velocity coupling. The flowfield is solved by the Eulerian scheme + LES turbulence model segregatedly. The whole simulations were taken as adiabatic thus, there were no attempts for also solving the energy equation or temperature. A convergence criterion of 10^{-5} has been applied for the numerical simulations.

3 Results and Discussion

The transient numerical sound attenuation predictions were conducted both for 50 dB and 65 dB inlet perturbing noise levels which correspond to 0,0063 Pa and 0,035 Pa pressure wave amplitudes respectively. The same predictions were replied for existing mean fluid flow. The resultant frequency responses have been plotted by Fast Fourier Transformation (FFT) applied on the pressure data.

The results for acoustical behaviour in the dominance of LES mean flowfield is given with the dimensionless parameters in order to further investigate the results. Dimensionless time is introduced as follows. t_s^* is the time step number which is also a dimensionless quantity and Δt is the time step size. c and Φ_i are the local speed of sound and the pipe inner diameter respectively.

$$t^* = \frac{t_s^* . \Delta t . c}{\Phi_i} \tag{10.1}$$

Reynolds number, Helmholtz number and Mach number are used in order to state the flow turbulence and the acoustical perturbation non-dimensional frequency. These dimensionless numbers may be used in order to further investigate the consequences of the filter design.

$$\mathrm{Re}_D = \frac{\rho . U . \Phi_i}{\mu}, \qquad He = \frac{\pi . f . \Phi_i}{c}, \qquad Ma = \frac{\bar{u}}{c} = \frac{\bar{u}}{\sqrt{kRT}} \tag{10.2}$$

3.1. Frequency responses without fluid mean flow

In order to make functional tests with the aid of numerical simulations a specific positioning for the filter assembly is chosen progressively. This depends on the difficulty of the number of cases with many different filter assembly orientations (tune positions) also with the variety of perturbation wave frequencies.

The aeroacoustic filter, with the proposed concept structure in this paper is able to be tuned at maximum filtering capabilities for a maximum of 7163 Hz and a minimum of 865 Hz for the first acoustic mode depending on the pathway difference calculations regarding to equation (1).

Table 2: Limiting tune positions and their relevant predicted filtering frequencies.

	In-Phase				Out of Phase			
m	***λ (m)***	***f (Hz)***	***λ (m)***	***f (Hz)***	***λ (m)***	***f (Hz)***	***λ (m)***	***f (Hz)***
0	0,3998	**865,4**	0,0966	3581,8	0,1999	**1730,9**	0,0483	7163,6
1	0,1333	2596,3	0,0322	10745,3	0,1000	3461,7	0,0242	14327,1
2	0,0800	4327,2	0,0193	17908,9	0,0666	5192,6	0,0161	21490,7
Orientation	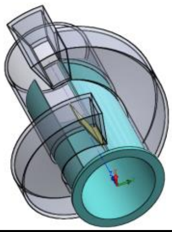		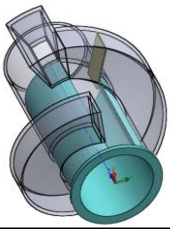		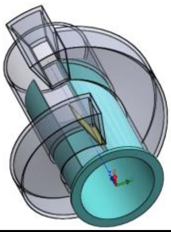		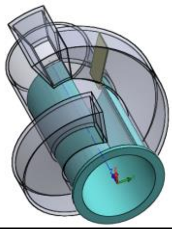	

The incoming perturbed sound waves preserve their peak-to-peak and normal-to-peak amplitudes until interacting with the EAF. The waves transmitted through the filter apparently loses amplitude. The below postprocessor results have all the same legend color value limits in order to make a visual inspection.

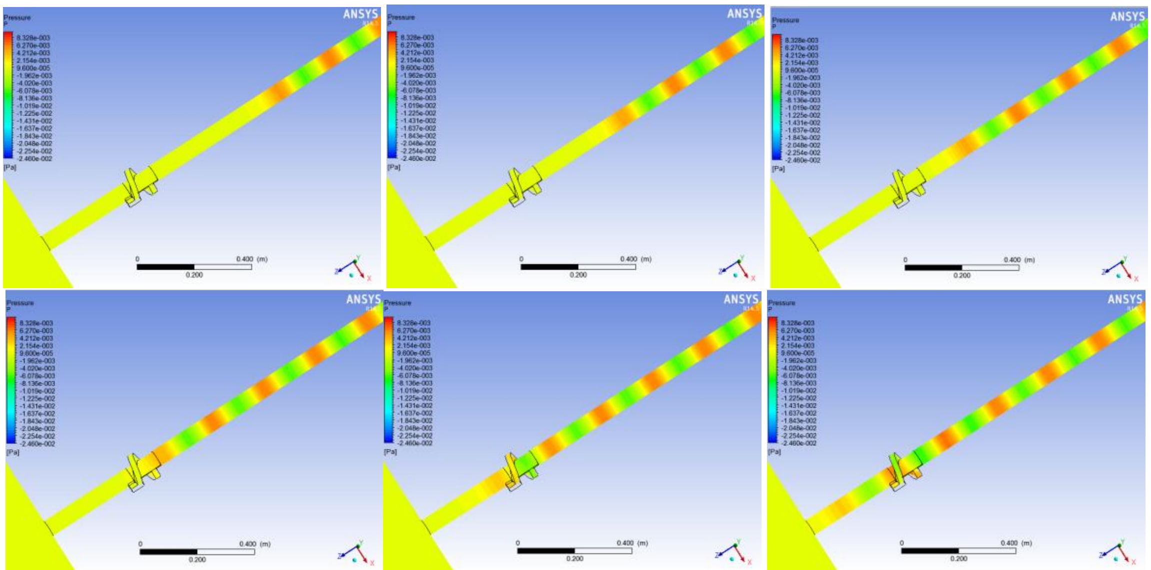

Figure 8.1: Pressure contours for 865 Hz and 50 dB (0,0063 Pa) perturbation: time evolves with constant increment.

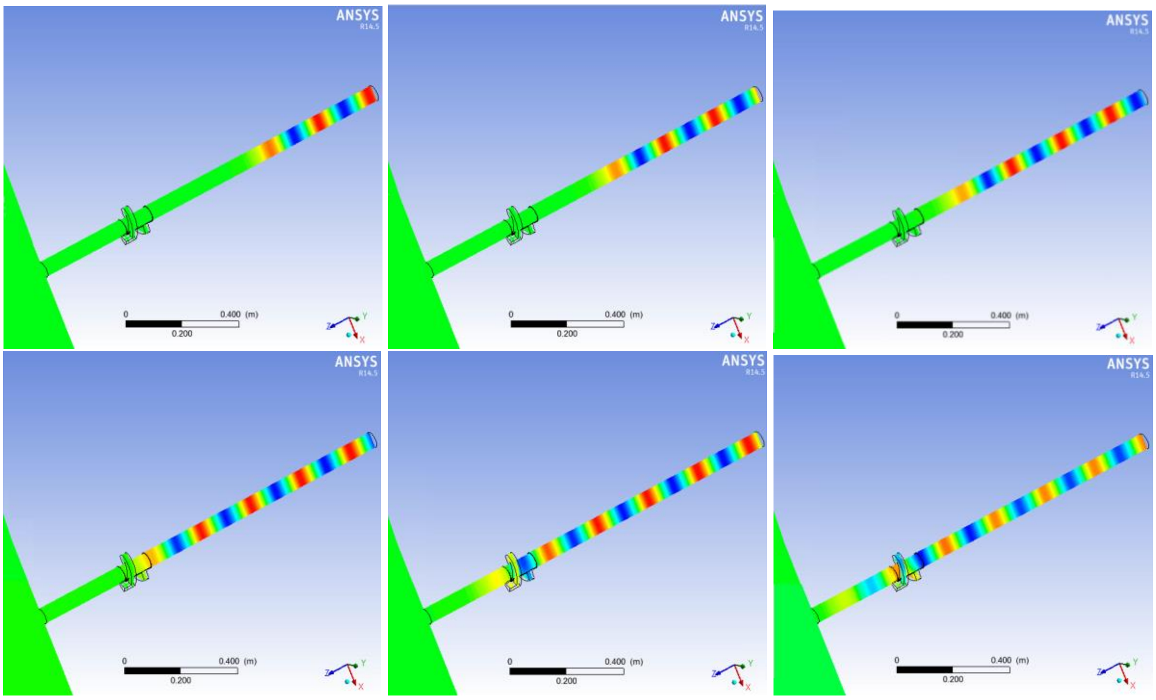

Figure 8.2: Pressure contours for 1730 Hz and 50 dB (0,0063 Pa) perturbation: time evolves with constant increment.

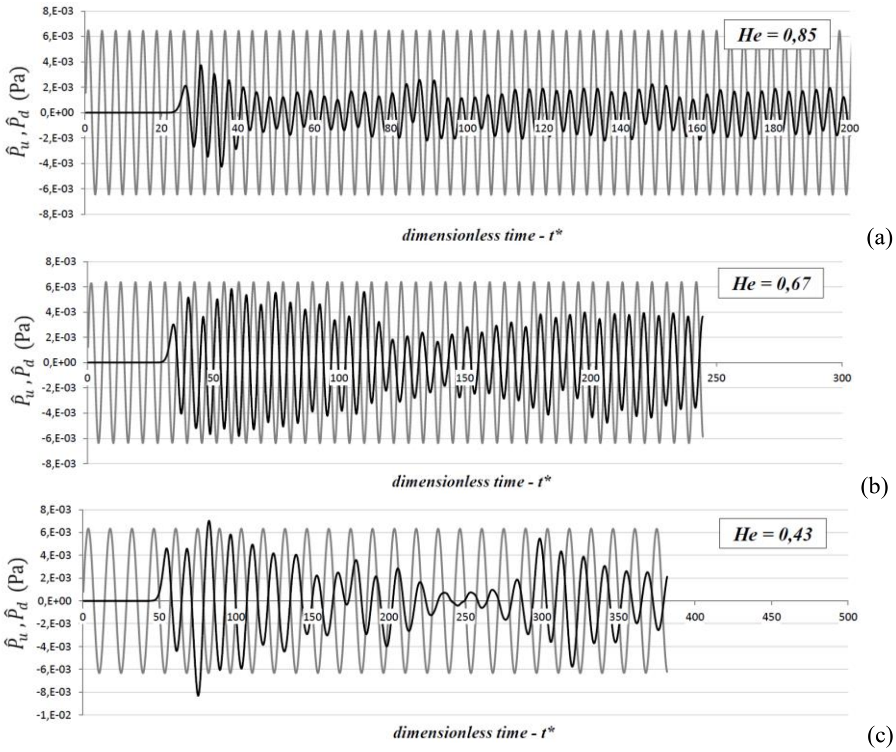

Figure 8.3: Pressure plots from monitoring upstream and downstream points with different Helmholtz numbers for 50 dB (0,0063 Pa), a) 1730 Hz, b) 1350 Hz and c) 865 Hz.

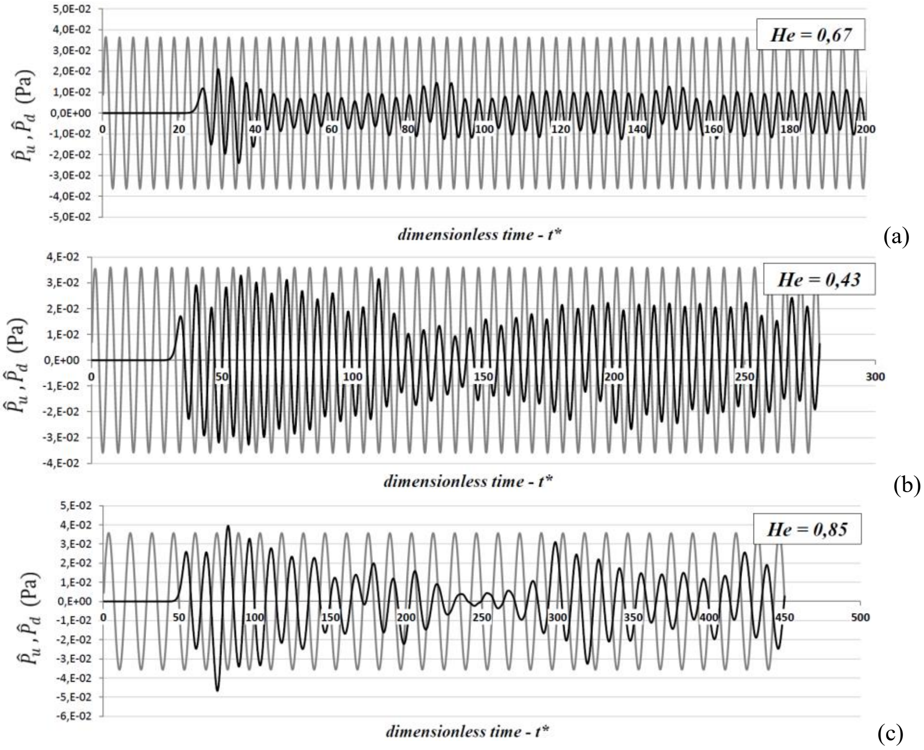

Figure 8.4: Pressure plots from monitoring upstream and downstream points with different Helmholtz numbers for 65 dB (0,035 Pa), a) 1730 Hz, b) 1350 Hz and c) 865 Hz.

The frequency spectrum of both the acoustical inlet (perturbing) waves' and the passed (transmitted) downstream waves' are calculated and displayed for different frequencies.

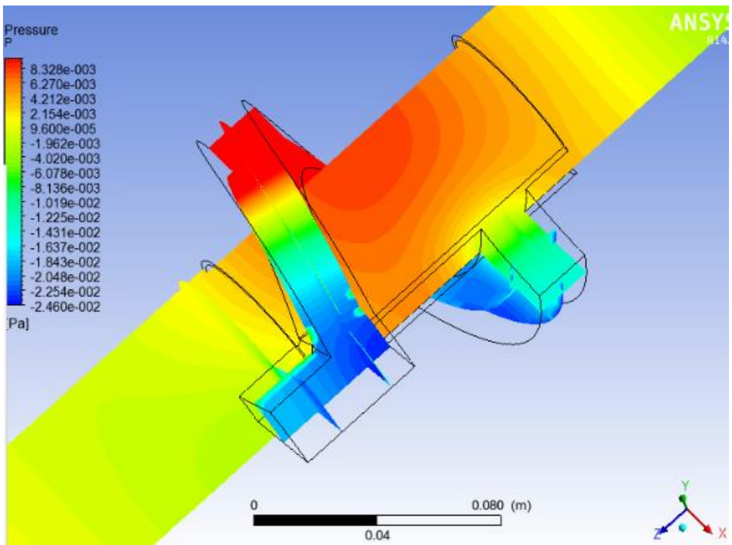

Figure 9: Sample pressure contour image from the flow domain and attenuation from the solver postprocessor.

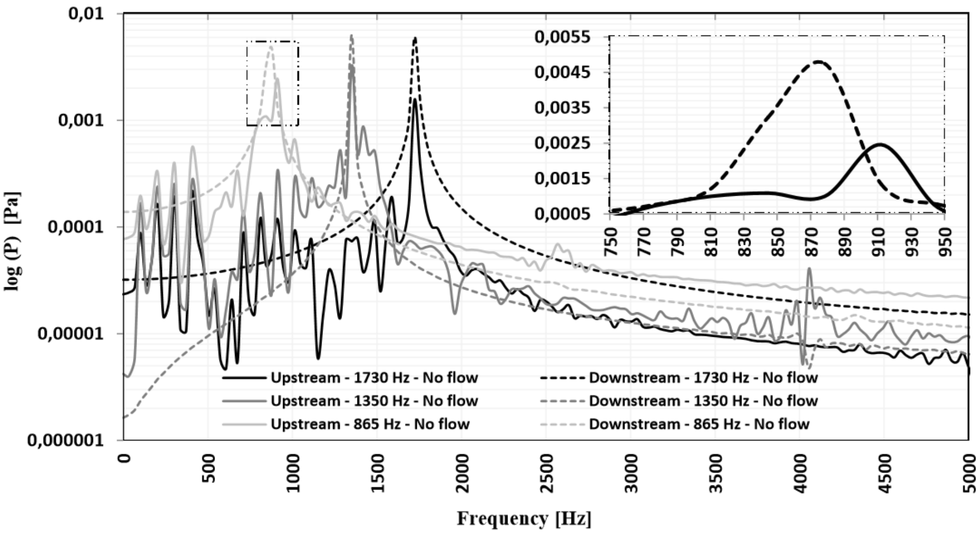

(a)

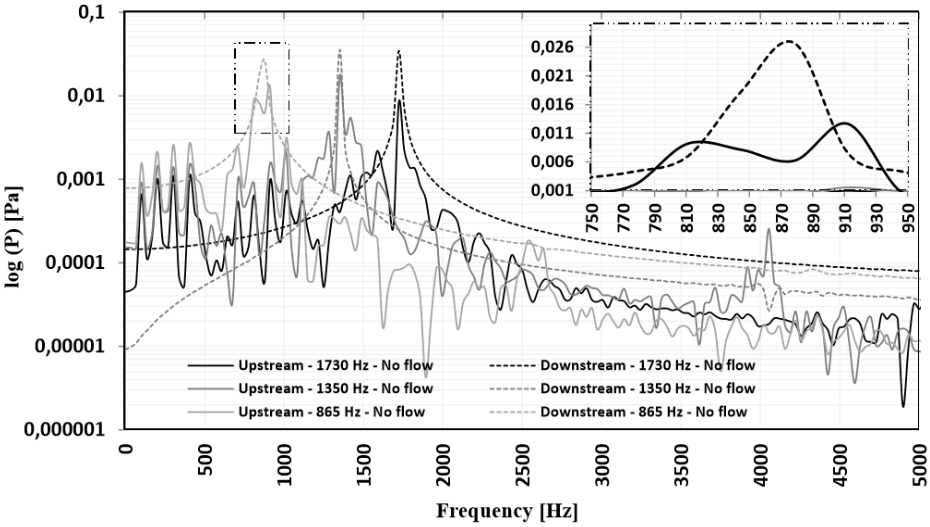

(b)

Figure 10: FFT plots for a) 50 dB, b) 65 dB perturbation without mean flow case.

When focusing attention on the 865 Hz and 1730 Hz regions, it is seen that the apparent transmission loss stands much greater than the 1350 Hz sample frequency. As talking about 1350 Hz FFT results, the relative transmission loss is significantly lower than the others. This should be due to non-correspondancy about an in-phase or an out of phase destructive interference which occured for 865 Hz and 1730 Hz. Thus this sample tune position is not the best tune position for 1350 Hz silencing etc. There is another position for getting the best result for 1350 Hz or any frequency of interest.

Table 3: Transmission loss values with respect to pressure peak values without mean flow.

	50 dB Perturbation			*65 dB Perturbation*		
f (Hz)	$\hat{p}'_u$ ***(Pa)***	$\hat{p}'_d$ ***(Pa)***	***TL (dB)***	$\hat{p}'_u$ ***(Pa)***	$\hat{p}'_d$ ***(Pa)***	***TL (dB)***
865	0,0047	0,0010	13,5	0,0267	0,0062	12,7
1350	0,0063	0,0033	5,7	0,0356	0,0175	6,2
1730	0,0061	0,0016	11,8	0,0346	0,0084	12,3

3.2. Frequency responses with fluid mean flow

The numerical simulations and data processing is as follows: First of all in CFD calculations, all of the simulation cases were initiated as a steady analysis under the dominance of LES turbulence model. The steady parts consists of converged LES flowfields in all cases. After then, converged LES datas are used to initiate the domain for transient aeroacoustic cases. In the aeroacoustic simulations, the converged flow field has been made evolve under pressure perturbation plus the fluid outflow. The acoustically emitted waves are planar type with coherent contraction or relaxation effect on the fluid media. Following the steady and converged LES data, the outlet velocity has been increased to the desired value of 6 m/s by a ramp function. 6 m/s is the maximum flow speed at full load of which the filter assembly is designed to be mounted on the air intake of the boiler. After achieving the maximum outflow speed, an additional time for turbulent wake formation has also been let to develop before the start of acoustic perturbation. The resultant aeroacoustic simulations were conducted by this procedure.

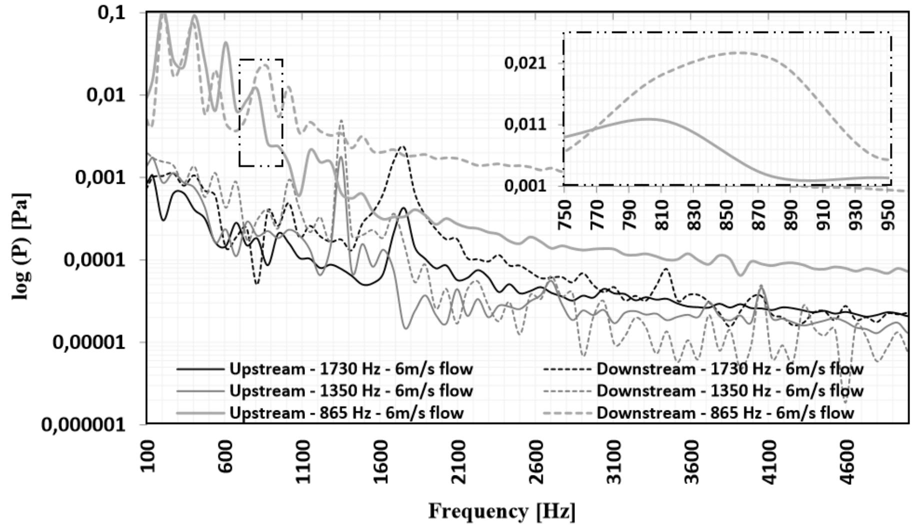

(a)

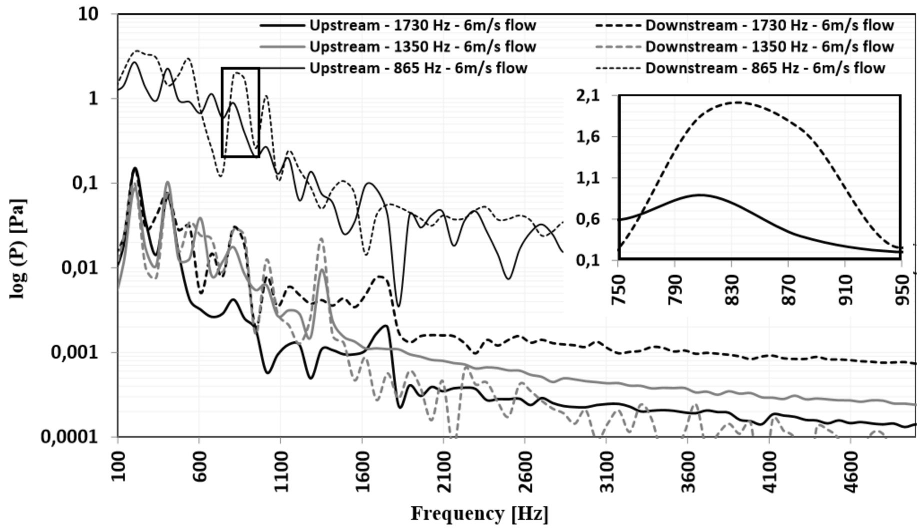

(b)

Figure 11: FFT plots for a) 50 dB, b) 65 dB perturbation with mean flow case.

The mean flow results have been filtered by occupying CBF methodology given in Section 2.2. When comparing the frequency vs. transmission loss values in Table 3 and Table 4, it is seen that the results are in correspondance which was aforementioned in the relative expected filtered frequencies with the corresponding filtering position in Table 2.

Table 4: Transmission loss values with respect to pressure peak values in case of mean fluid flow.

				50 dB Perturbation			***65 dB Perturbation***		
f (Hz)	***He***	***Re***	***Ma***	$\hat{p}_u^{'}$ ***(Pa)***	$\hat{p}_d^{'}$ ***(Pa)***	***TL (dB)***	$\hat{p}_u^{'}$ ***(Pa)***	$\hat{p}_d^{'}$ ***(Pa)***	***TL (dB)***
865,0	0,43	$2{,}079 \times 10^4$	0,017	0,0217	0,0026	18,5	1,6972	0,3939	12,7
1350,0	0,67	$2{,}079 \times 10^4$	0,017	0,0049	0,0018	8,9	0,0220	0,0095	7,3
1730,0	0,85	$2{,}079 \times 10^4$	0,017	0,0023	0,0004	14,7	0,0068	0,0020	10,8

As stated in Eq (9), the real part of the acoustic impedance stands for the acoustical resistance which is equal to **Re**(-*C12*). Evaluating the processed results, a time history for resistance to attenuation is achieved both for 50 dB and 65 dB perturbing inlets. Regarding the similarity of the attenuated perturbation characteristics given the result for 65 dB in Figure 12.

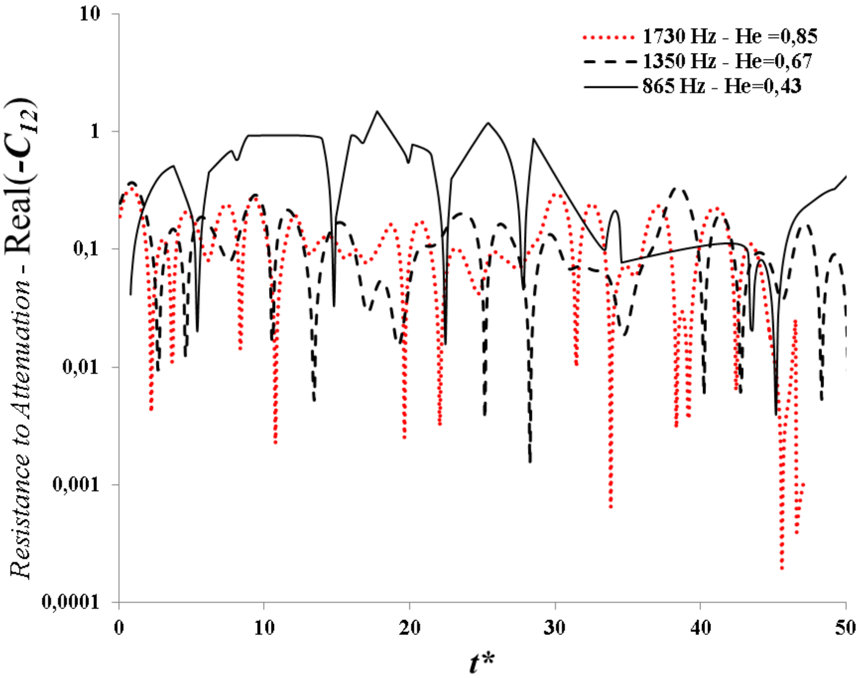

Figure 12: Resistance to 65 dB perturbation attenuation v.s. dimensionless time.

The results point out a successful operation. There is correspondance between the calculated and the expected results talking about the frequencies of interest.

It is an apparent expectation from a fundamental mechanism of nature that, any magnitude of successive destructive interference should have been validated by the proposed sound filtering method in this paper. The important issue is, whether it can be due to decreasing or increasing effects, the most successful transmission losses are approved by the numerical results. They are in successive correlation with the geometrical desctructive interference expectation.

4 Conclusions

The maximum predicted filtering performance has been validated numerically for both 50 dB and 65 dB incident perturbation and for both only acoustics and acoustics + flow conditions. Different transmission losses have been calculated from the achieved results. This filtering performance is also supplied with the advantage and ability of no counteraction on fluid flow (like pressure losses) inside the duct. Shape parameters and their effect on the bandwidth of filtering accuracy and experimental validation can be issued as a futurework.

Acknowledgement

We would like to thank Prof. Dr. İ. Bedii Özdemir for the valuable effect, knowledge and initiation that he has given to our will about this work.

References

[1] S. Föller and W. Polifke. Identification of aero-acoustic scattering matrices from large eddy simulation. Application to a sudden area expansion of a duct. J. Sound & Vib. (JSV), 331:3096-3113. DOI: 10.1016/j.jsv.2012.01.004

[2] F. A. Everest. *The Master Handbook of Acoustics*, Fourth Edition. Mc-Graw Hill. 2001. DOI: 10.1036/0071399747

[3] F. M. White. *Viscous Fluid Flow.* 2nd Edition. McGraw-Hill. 1991. ISBN 0-07-069712-4.

[4] J. Blauert and N. Xiang. *Acoustics for Engineers.* Springer. 2008. DOI: 10.1007/978-3-540-76348-2

[5] J. Kopitz, E. Bröcker and W. Polifke. Characteristics-based filter for identification of planar acoustic waves in numerical simulation of turbulent compressible flow. ICSV12, Twelfth International Congress on Sound and Vibration, 11-14 July 2005, Lisbon.

[6] J. M. Middelberg, T. J. Barber, S. S. Leong, K. P. Byrne and E. Leonardi. Computational fluid dynamics analysis of the acoustic performance of various simple expansion chamber mufflers. Proceedings of ACOUSTICS, 3-5 November 2004, Gold Coast, Australia.

[7] ANSYS, Inc. 2006. *ANSYS-CFX Solver Theory Guide.*

[8] D. Noreland. Impedance boundary conditions for acoustic waves in a duct with a step discontinuity. Technical Report – Department of Information Technology, Uppsala University. 2003.

[9] S. Dykas, W. Wróblewski, S. Rulik and T. Chmielnak. Numerical method for modeling of acoustic waves propagation. Arch. Acoust., 1, 35-48 (2010). DOI: 10.2478/v10168-010-0003-7

[10] Y. Hwang, J. M. Lee, S. Kim. New active muffler system utilizing destructive interference by difference of transmission paths. Journal of Sound and Vibration 262 (2003) 175-186. DOI: 10.1016/S0022-460X(02)01378-0